Supporting information for

Oxidation of Mn(III) Species by Pb(IV) Oxide as a Surrogate Oxidant in Aquatic Systems

Xingxing Wang[1], Qihuang Wang[1], Peng Yang[2], Xiaoming Wang[3], Liwu Zhang[1,4], Xionghan Feng[3], Mengqiang Zhu[2], Zimeng Wang[1,4]*

[1]Department of Environmental Science and Engineering, Fudan University, Shanghai, China

[2]Department of Ecosystem Science and Management, University of Wyoming, Laramie, Wyoming, United States

[3]College of Resources and Environment, Huazhong Agricultural University, Wuhan, China

[4]Shanghai Institute of Pollution Control and Ecological Security, Shanghai, China

*Corresponding author: zimengw@fudan.edu.cn

Website: zimengwang.org.cn

Environmental Science & Technology

24 Pages, 4 Text Sections, 13 Figures, 4 Tables,

Contents **Page**

Text 1 Detail information of the batch experiments

All experiments were conducted with 200 mL solution volume in 250 mL borosilicate glass bottles with polypropylene caps. All bottles were wrapped with aluminum foil to prevent the potential interference by the light. Specific volumes of 50 mM PP stock solution were added to deionized water to achieve the desired concentration of the experimental solutions summarized in Table S1. Then, the solution pH was adjusted to desired values with 0.1 M NaOH or 0.1 M HNO_3. Excess PP served as a pH buffer (pK_a = 0.9, 2.0, 6.6, 9.4).[1] This method of pH control worked well for all Mn(II) and dissolved Mn(III) systems.[2] For experiments without PP, 10 mM MOPS (3-(N-morpholino) propanesulfonic acid, pK_a = 7.2) was used as pH buffer. Next, various manganese-containing substances were added to this solution. If necessary, 0.1 M NaOH and 0.1 M HNO_3 were added again for pH adjustment. Finally, PbO_2 was added to the solutions. It is worth noting that Mn(III)−PP stock solution was added after the addition of PP to prepare different solutions for the experiment, instead of the reverse order, to prevent the disproportionation of Mn(III). For all batch experiments, the reactors were completely mixed with magnetic stir bars (500 rpm) on magnetic stirrers (RO 15, IKA, Germany) at room temperature (23±1 ℃).

Text 2 Detail information of the solid characterization methods

Raman spectroscopy. Raman spectra were collected with a XploRA Plus confocal Raman spectrometer (Jobin Yvon, Horiba Gr, France). The samples were excited by a laser beam at 785 nm emitted by an external-cavity diode with a power of 9 mW. A 50x Olympus microscope objective with numerical aperture of 0.5 focused the laser beam to about 2 μm diameter on the sample. Instrumental precision was calibrated against the Stokes Raman signal of pure Si at 520 cm^{-1} using a silicon wafer (110). The detector was a multichannel charge-coupled Device (CCD) equipped with a 1200 lines per mm diffraction grating. Every spectrum was obtained by averaging 3 accumulations at a 10s acquisition time. The spectroscopy software LabSpec 6 Software (Jobin Yvon, Horiba Gr, France) was used to manipulate the spectra.

Scanning Electron Microscopy (SEM) and Energy Dispersive X-ray Spectroscopy (EDX). A TESCAN VEGA 3 SBU scanning electron microscope (TESCAN Ltd., Brno, Czech Republic) equipped with an energy-dispersive X-ray detector (XFlash detector 610 M, Brucker Nano GmbH, Germany) was used for morphological evaluation of particles and elements analysis. The images were collected at the voltage of 15 kV or 10 kV. The powder sample was dispersed on a sticky carbon tape for SEM and EDX measurements. To calculate the atomic ratio (atomic %) of elements, the carbon

indexing was removed while performing the EDX analysis because the C signal for this kind of inorganic sample generally comes from the contamination caused by the air in the sample surface.

X-ray photoelectron spectroscopy. X-ray photoelectron spectroscopy (XPS) was conducted on a Thermo ScientificTM K-AlphaTM+ spectrometer equipped with a monochromatic Al *K*α X-ray source (1486.6 eV) operating at 100 W. Samples were analyzed under vacuum (P < 10−8 mbar) with a pass energy of 150 eV (survey scans) or 25eV (high-resolution scans). All peaks were calibrated with C1s peak binding energy at 284.8 eV for adventitious carbon. The experimental peaks were fitted by using Avantage software with the Gaussian−Lorentzian function (70% G-30% L), and Shirley background was used for peak fitting. The quantification of Mn valence state was made following a method in which the Mn $2p_{3/2}$ spectrum is divided into five multiplet peaks (total of 15 binding energies) of Mn(IV), Mn(III), and Mn(II)[3]. A value of 1.25 for the full width of the peak at half the maximum peak height (FWHM) was assigned to fit the Mn $2p_{3/2}$ spectrum for all of the multiplet binding energy spectra[4].

Text 3 Detail information of the thermodynamic database

The "thermo_ladder" file, published by Bethke et al[5] as a peer-reviewed thermodynamic database, was used as the basis of the calculations, within which PP^{4-} was added as a component species with multiple protonated species with different pK_a values. Redox and hydrolysis reactions of PP species were suppressed for their slow kinetics in abiotic systems.[6] The Mn(III)-PP complex, defined as $Mn(PP)_2^{5-}$ in our previous study,[2] was also considered in the present calculations. Mn oxide mineral species that rarely form at ambient temperatures including pyrolusite and bixbyite were suppressed.[7, 8] The formation kinetics of todorokite under ambient temperature are very slow[9], so it was also suppressed. The calculations utilized birnessite ($Mn_8O_{19}H_{10(s)}$) as an analog of the solid product for its average valance state of Mn (~3.5), as noted in the main text and also in our previous work.[2] Key equilibrium reactions and constants relevant to the thermodynamic calculations were listed in Table S4.

Text 4 The calculation of electron balance and reaction stoichiometry

For redox reactions between Mn(II) and PbO_2 in the presence of PP, the electron donor is Mn(II), and its oxidized products are Mn(III) and Mn oxides. The electron acceptor is PbO_2 and its reduced product is Pb(II). We can determine the reaction stoichiometry with electron conservation rules.

Taking the 10:1 ratio as an example (Figure S2b, exp 8), if we referred to 3.5 as the Mn AOS in the solid product and used the loss of total dissolved Mn to represent the quantity of Mn oxide solids, then the 3-hour duration produced 27 μM Mn oxides and 15 μM Mn(III), equivalent to 55.5 μM electron donated by Mn(II). This value perfectly matched the released 27 μM Pb(II) for electron balance. This consistency was observed throughout the entire duration of the experiments (Figure S 11b). A similar relationship between electron transfer amounts in Mn and Pb was also found in other experiments throughout the entire duration of our study (Figure 3).

While Mn(II) was rapidly consumed, the intermediate Mn(III) reached a maximum of 15 μM in 3 hours and then took over 100 hours to decrease to 5 μM. In line with the decrease of total dissolved Mn that indicated the formation of solid phase Mn, the dissolved Pb also further increased to an extent of nearly 1/4 of that of Mn(III) consumption. The second stage was likely the Mn(III) oxidation by PbO_2 that continued to release Pb at a slower rate.

Based on the above discussion, a conceptual model of the reaction between PbO_2 and Mn(II) and Mn(III) in the presence PP or in the absence of PP was proposed as shown in graphical abstract.

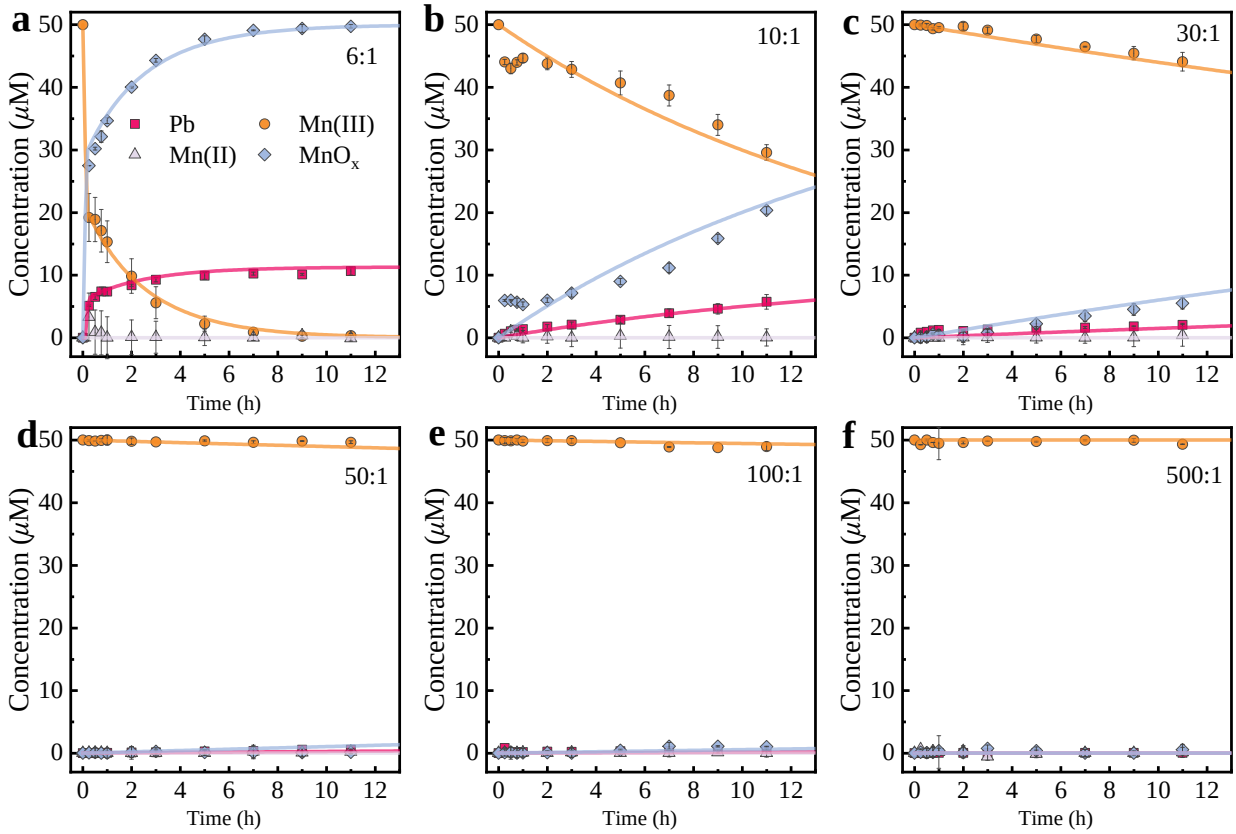

Figure S1. Batch experiments of 50 μM PbO_2 dissolution at pH 7 with different PP:Mn(III) ratios. The concentration of Mn(III) was fixed at 50 μM, and the concentration of PP was 300 μM, 500 μM, 1500 μM, 2500 μM, 5000 μM, and 25000 μM, respectively (exps 1–6 for panels a–f). The concentration of Mn(II) was calculated by subtracting the measured concentration of dissolved Mn(III)-PP from the concentration of total dissolved Mn. The concentration of MnO_x was represented by the loss of dissolved Mn. Experimental data and model simulations are shown as symbols and lines, respectively. Error bars indicate standard deviation from duplicate experiments. Propagation of error would cause some error bar could exceed the zero line.

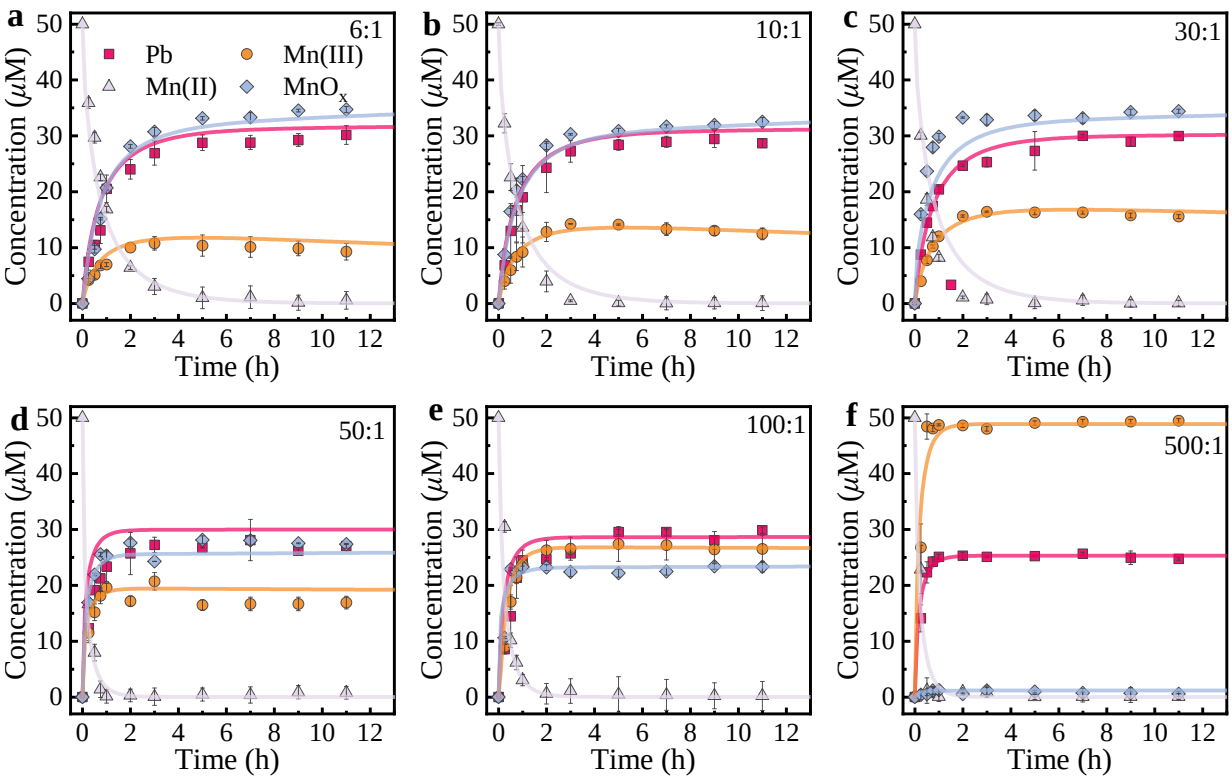

Figure S2. Batch experiments of 50 μM PbO_2 dissolution at pH 7 with different ratios of PP to Mn(II). The concentration of Mn(II) was fixed at 50 μM, and the concentration of PP was 300 μM, 500 μM, 1500 μM, 2500 μM, 5000 μM, and 25000 μM respectively (exps 7−12 for panels a−f). The concentration of Mn(II) was calculated by subtracting the measured concentration of dissolved Mn(III)-PP from the concentration of total dissolved Mn. The concentration of MnO_x was represented by the loss of dissolved Mn. Experimental data and model simulations are shown as symbols and lines, respectively. Error bars indicate standard deviation from duplicate experiments. Propagation of error would cause some error bar could exceed the zero line.

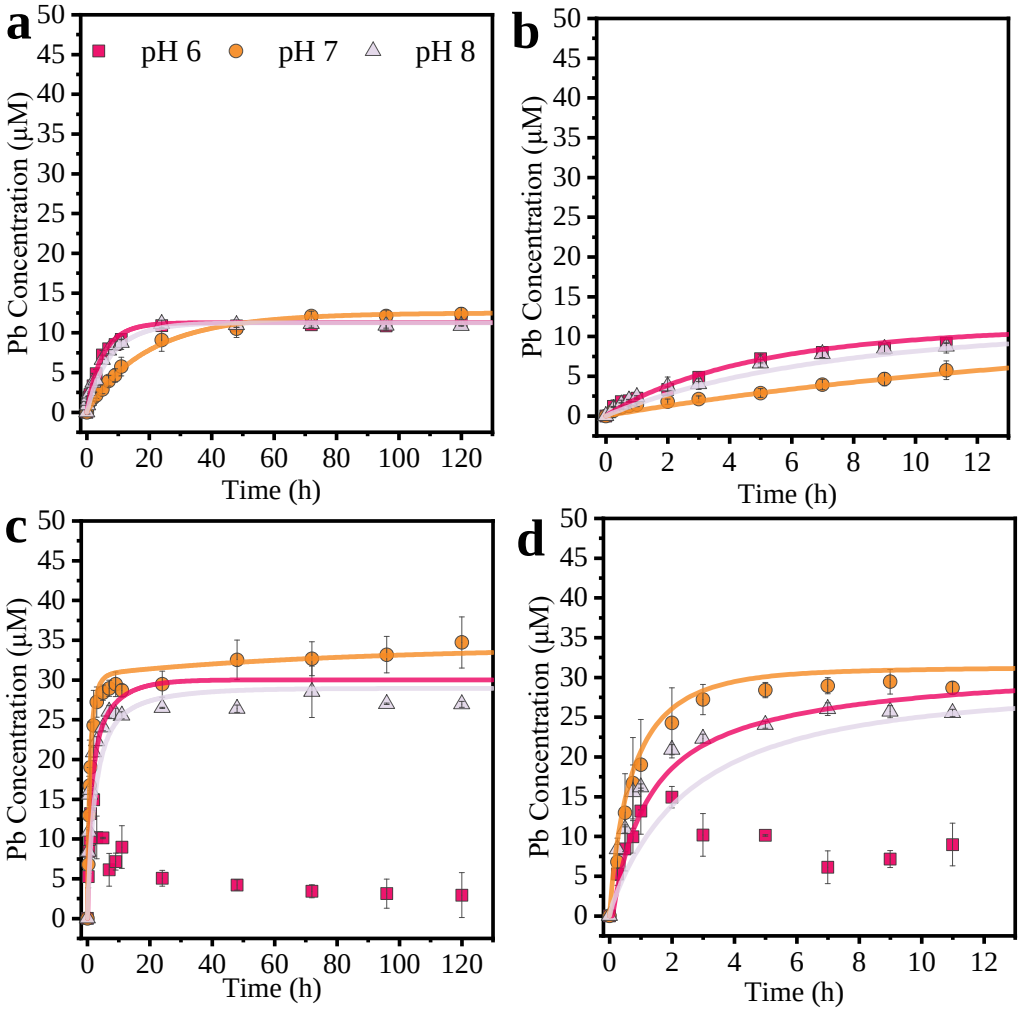

Figure S3. Effects of pH on the reduction of PbO_2 by dissolved Mn(III)-PP (a, exps 2, 15, and 16) and Mn(II) (c, exps 8, 17, and 18) in the presence of PP. Panel (b) and (d) provide an enlarged view of the initial stage of the reaction in Panel (a) and (c), respectively. Error bars indicate standard deviation from duplicate experiments.

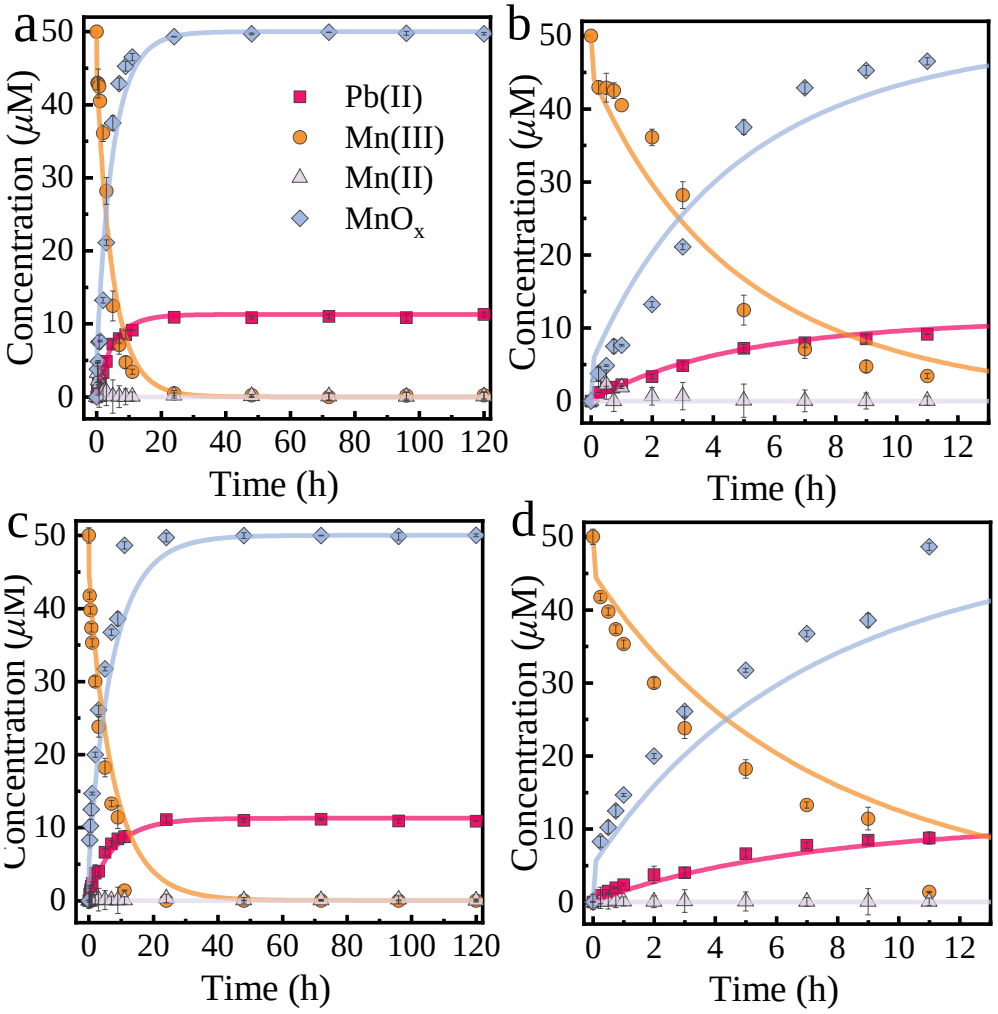

127

128 **Figure S4.** Batch experiments of PbO_2 dissolution at pH 6 (a, exps 15) and pH 8 (c, exp 16) in the presence of
129 Mn(III)-PP. Panel (b) and (d) provide an enlarged view of the initial stage of the reaction in Panel (a) and (c),
130 respectively. Error bars indicate standard deviation from duplicate experiments. Propagation of error would
131 cause some error bar could exceed the zero line.

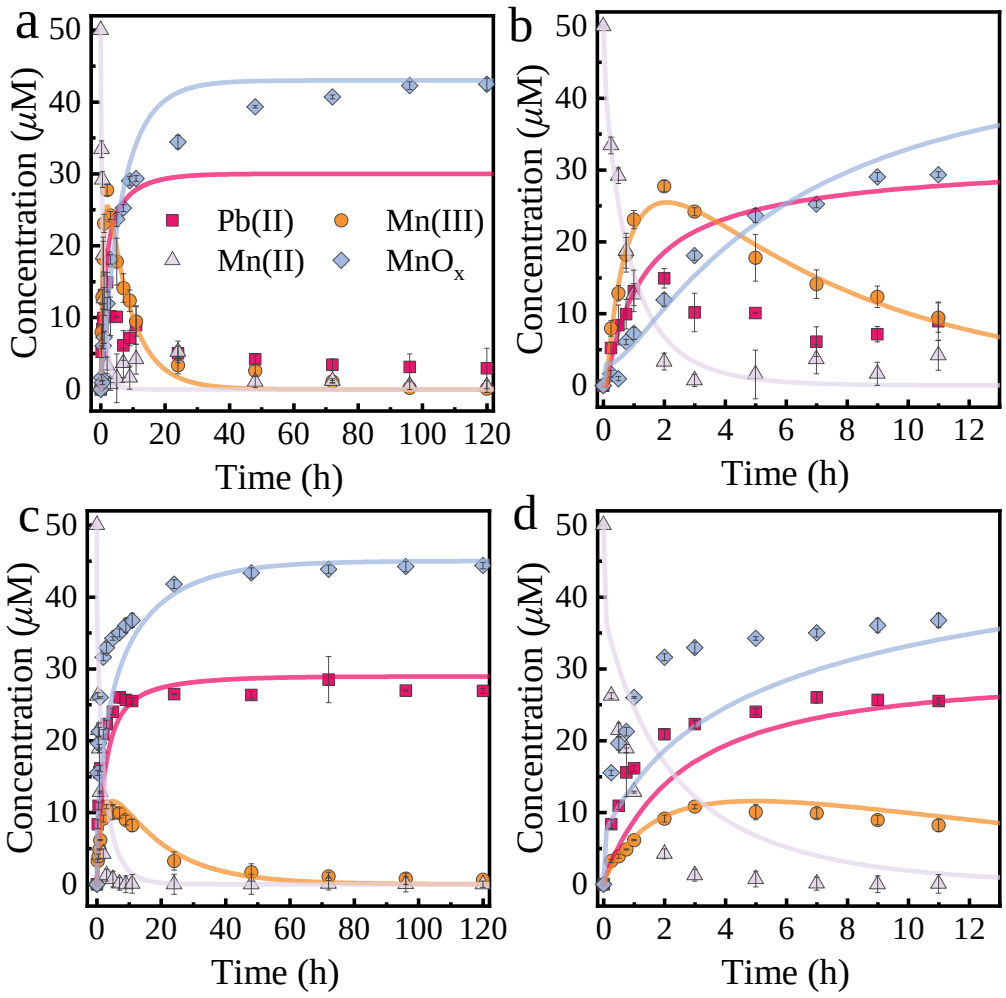

Figure S5. Batch experiments of PbO_2 dissolution at pH 6 (a, exp 17) and pH 8 (b, exp 18) in the presence of Mn(II) and PP. Panel (b) and (d) provide an enlarged view of the initial stage of the reaction in Panel (a) and (c), respectively. Error bars indicate standard deviation from duplicate experiments. Propagation of error would cause some error bar could exceed the zero line.

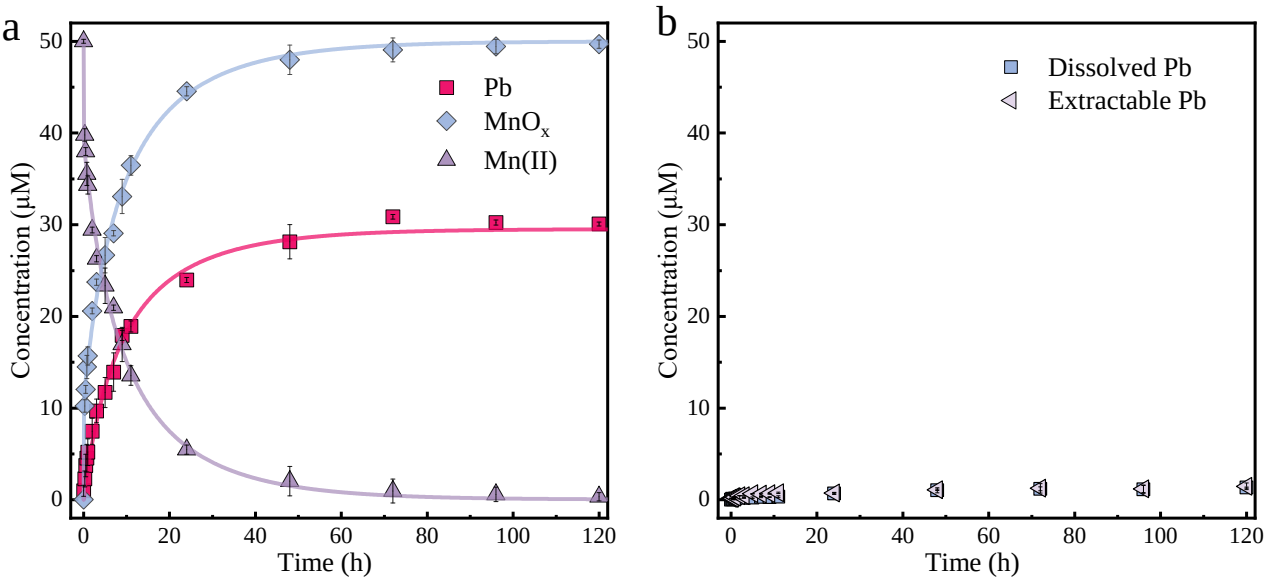

137

138 **Figure S6.** Batch experiments of PbO_2 dissolution in the presence of only Mn(II) (a, exp 20) and only PP (b,
139 exp 19). Error bars indicate standard deviation from duplicate experiments. Propagation of error would cause
140 some error bar could exceed the zero line.

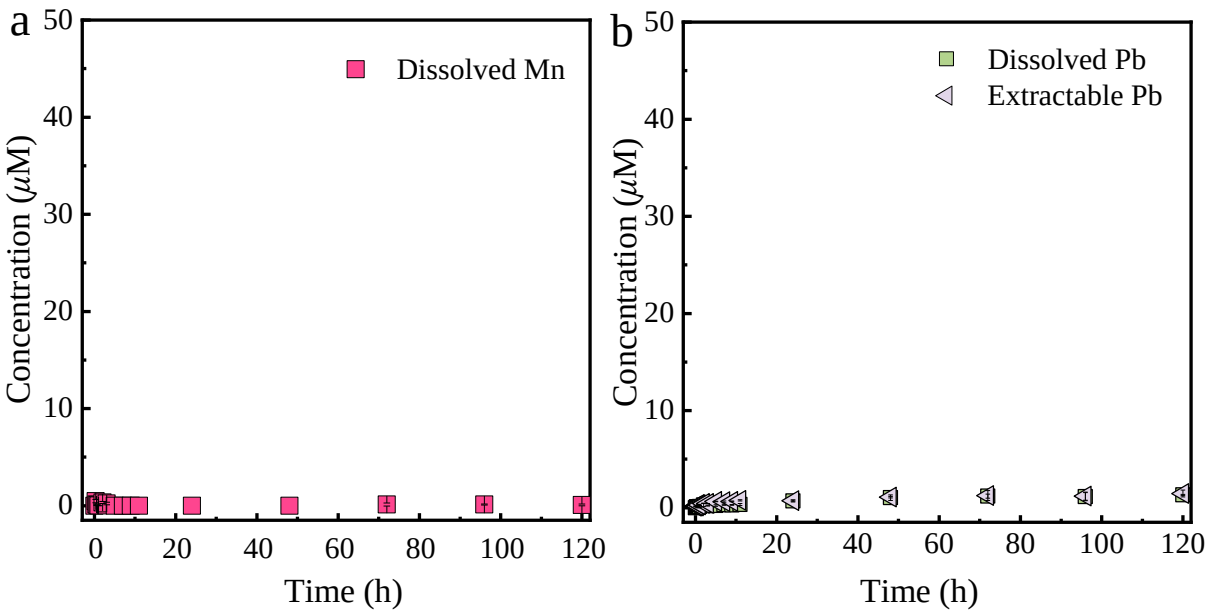

Figure S7. Batch experiments of only γ-MnOOH (a, exp 21) and only PbO_2 (b, exp 22). Extractable Pb values represent the total amount of dissolved Pb(II), including the amount adsorbed to the surface of PbO_2. Error bars indicate standard deviation from duplicate experiments. Propagation of error would cause some error bar could exceed the zero line.

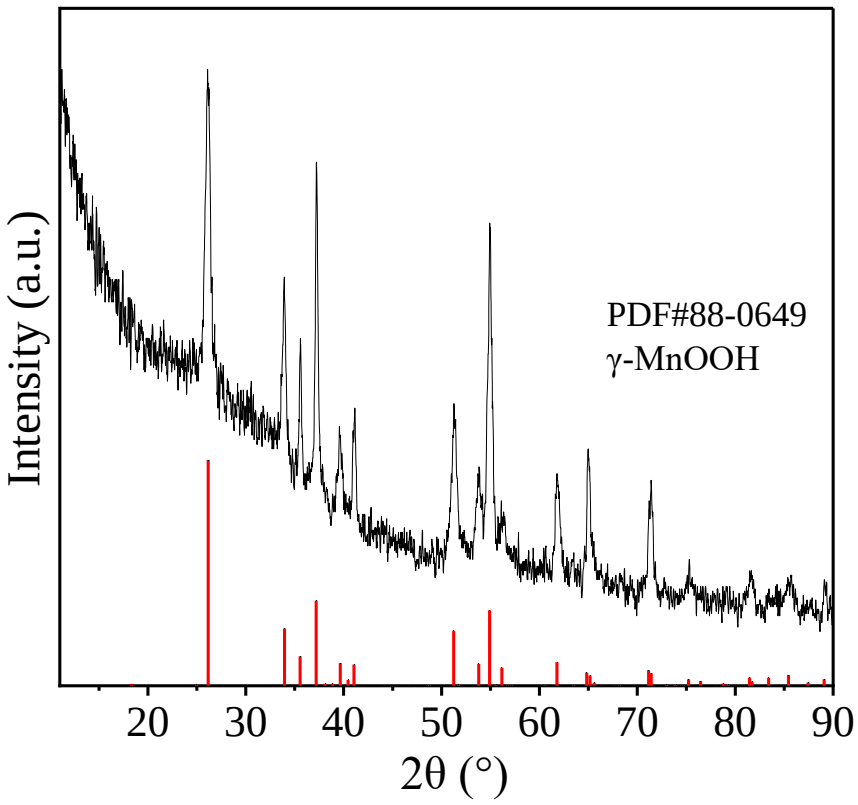

146

147 **Figure S8.** XRD patterns of the original manganite sample.

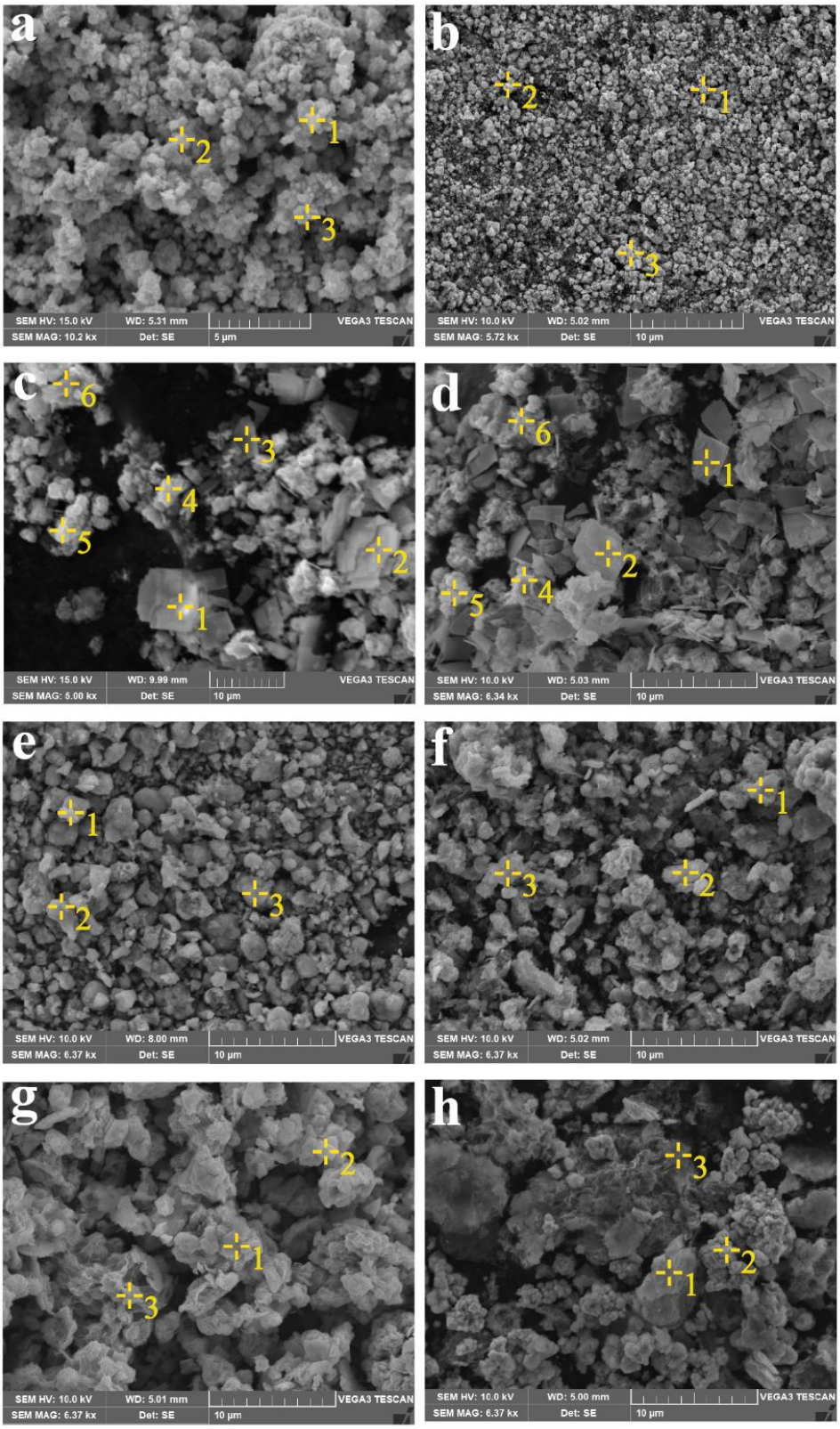

Figure S9. SEM images of experimental solids in different pH conditions with 1:10 ratio of PP:Mn(III)/Mn(II). (a) original PbO_2; (b) solids in control experiment with only PbO_2 (exp 22); (c) solids in pH 6 with Mn(II) (exp 17); (d) solids in pH 6 with Mn(III) (exp 15); (e) solids in pH 7 with Mn(II) (exp 8); (f) solids in pH 7 with Mn(III) (exp 2); (g) solids in pH 8 with Mn(II) (exp 18); (h) solids in pH 8 with Mn(III) (exp 16). The numbers in the images showed the selected point of EDS analyses (Table S3).

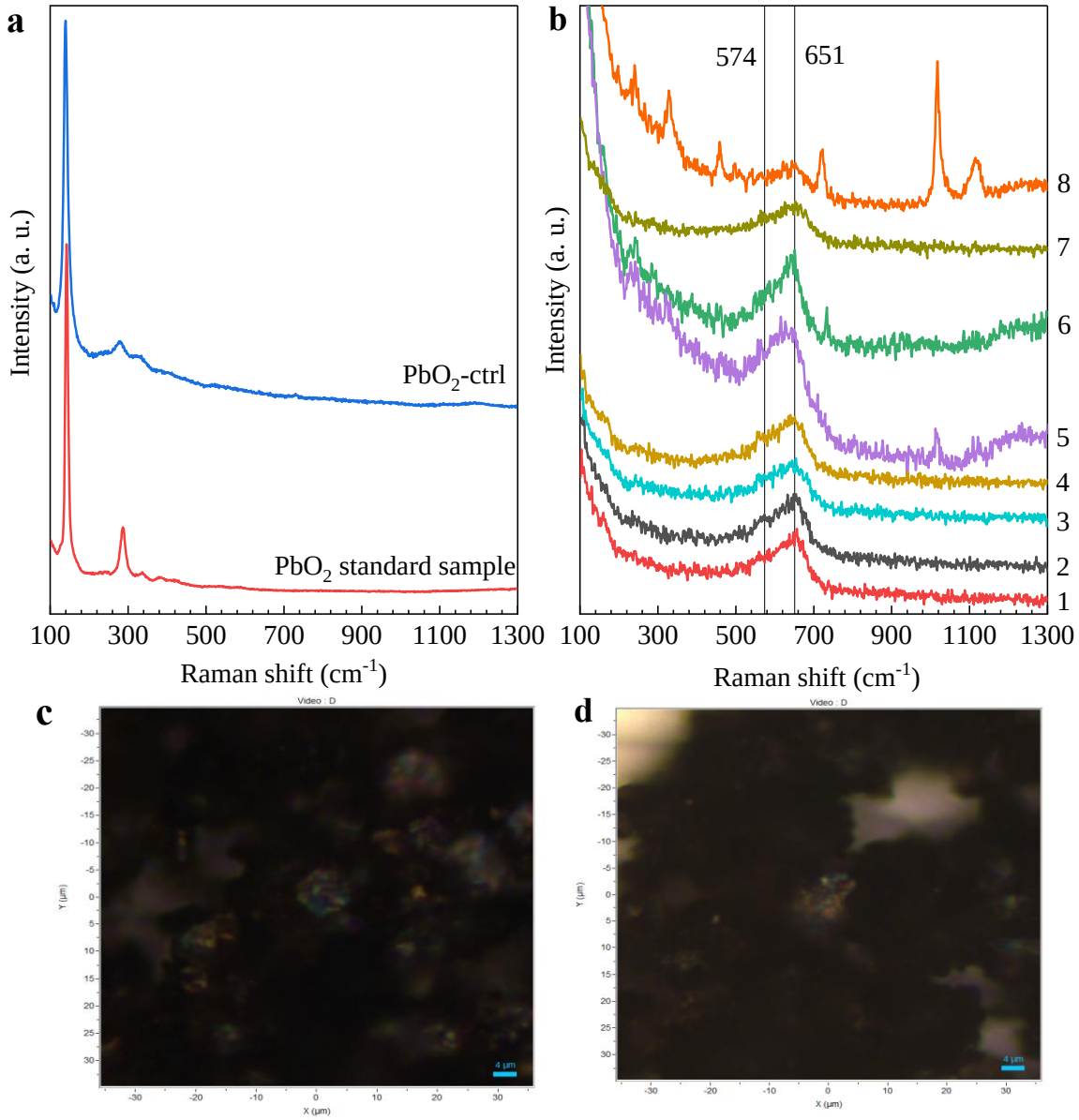

Figure S10. Raman spectra of the solids in control experiment with only PbO_2. (a) The solids of the experiments in different pH with 1:10 ratio of PP:Mn(II)/Mn(III) (b, line 1. in pH 7 with Mn(III) (exp 2); line 2. in pH 8 with Mn(III) (exp 16); line 3. in pH 7 with Mn(II) (exp 8); line 4. in pH 8 with Mn(II) (exp 18); line 5. in pH 6 with Mn(III) (exp 15); line 6. in pH 6 with Mn(III) (exp 15); line 7. in pH 6 with Mn(II) (exp 17); line 8. in pH 6 with Mn(II) (exp 17)). Optical microscope photographs in panels c and d showed the solid samples in pH 6 with Mn(II) and Mn(III), respectively. The two samples both have two different kinds of products, metallic and black areas, shown in (c) and (d), which correspond to lines (5-8) in panel b.

Optical microscope photograph provided by Raman spectrometer showed two different kinds of products in the experiments at pH 6, which were also found in SEM images (Figures S9 c, d). The peaks at 240, 328, 458, 723, 1016, and 1116 cm^{-1} in line 8 (Figure S10b) indicated the formation of lead pyrophosphate ($Pb_2P_2O_7$).[10] The peaks at 574 and 651 cm^{-1} showed the presence of layered Mn oxides,[11] and the peak profile and position was almost identical with that of birnessite documented by Julien et. al.[12]

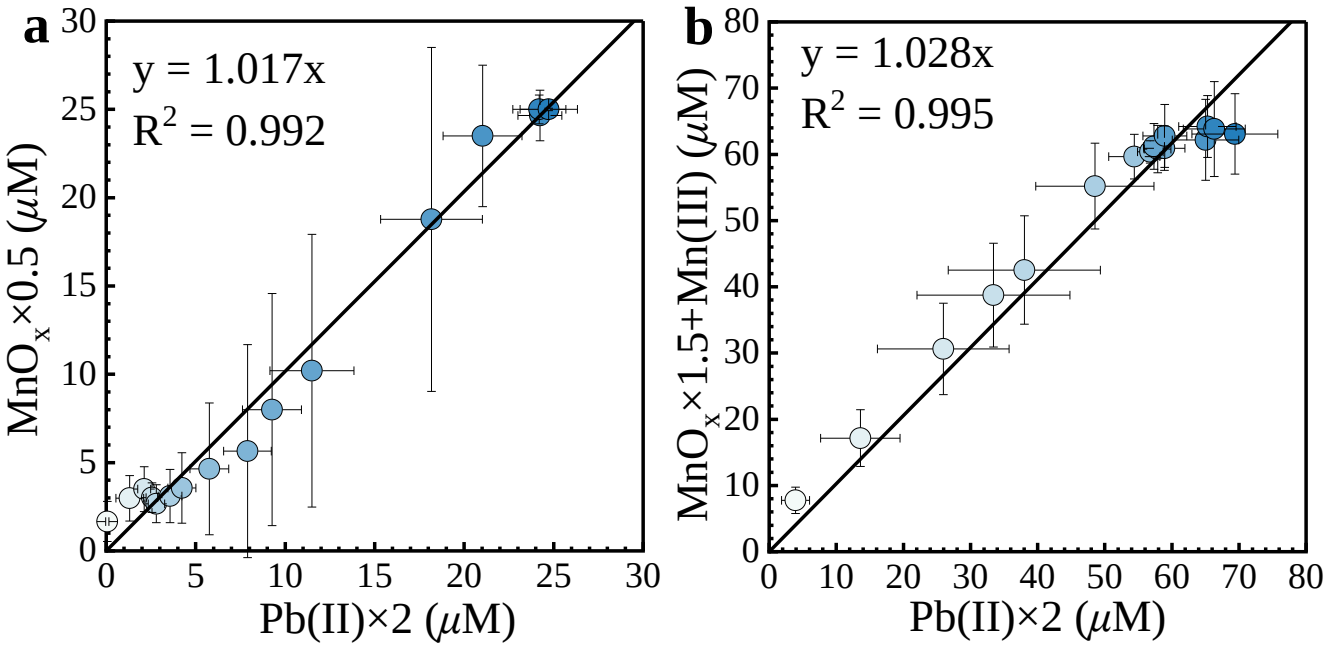

168

169 **Figure S11.** The correlation between the amount of electron transfer between the oxidant (PbO_2 → Pb(II)) and
170 reductant (Mn(III)→MnO_x; Mn(II)→Mn(III), MnO_x) throughout the experiments with (a, exp 2) 10:1 PP:Mn(III)
171 and (b, exp 8) 10:1 PP:Mn(II). A presumed Mn AOS of the produced MnO_x of 3.5 was used in the calculations.
172 In principle, Mn(III) should lose 0.5 moles of electrons when 1 mole of Mn oxides (MnO_x) are produced, while
173 PbO_2 should gain 2 moles of electrons for every 1 mole of Pb(II) produced. Mn(II) lost 1 mole and 1.5 moles
174 of electrons for every mole of Mn(III) and Mn oxide (MnO_x) produced, respectively. The uncertainty associated
175 with each data point was calculated considering error propagation. Propagation of error would cause some error
176 bar could exceed the zero line.

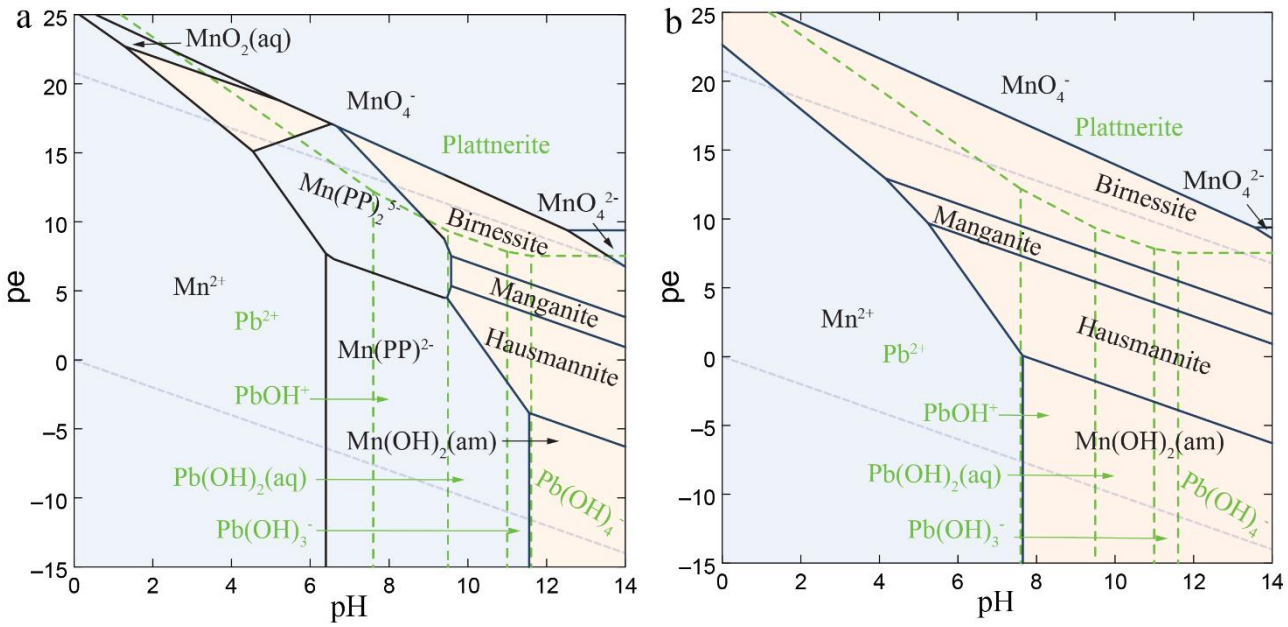

Figure S12. Two pe-pH diagrams of (a) Pb−Mn−PP and (b) Pb−Mn at 25 °C and 1 bar total pressure. Predominance areas were calculated for conditions with 25 μM Mn, 6.25 μM Pb, and 500 μM PP. Boundaries of predominance areas are shown for manganese (black) and lead (green) species. Light grey lines indicate the stability limits of water.

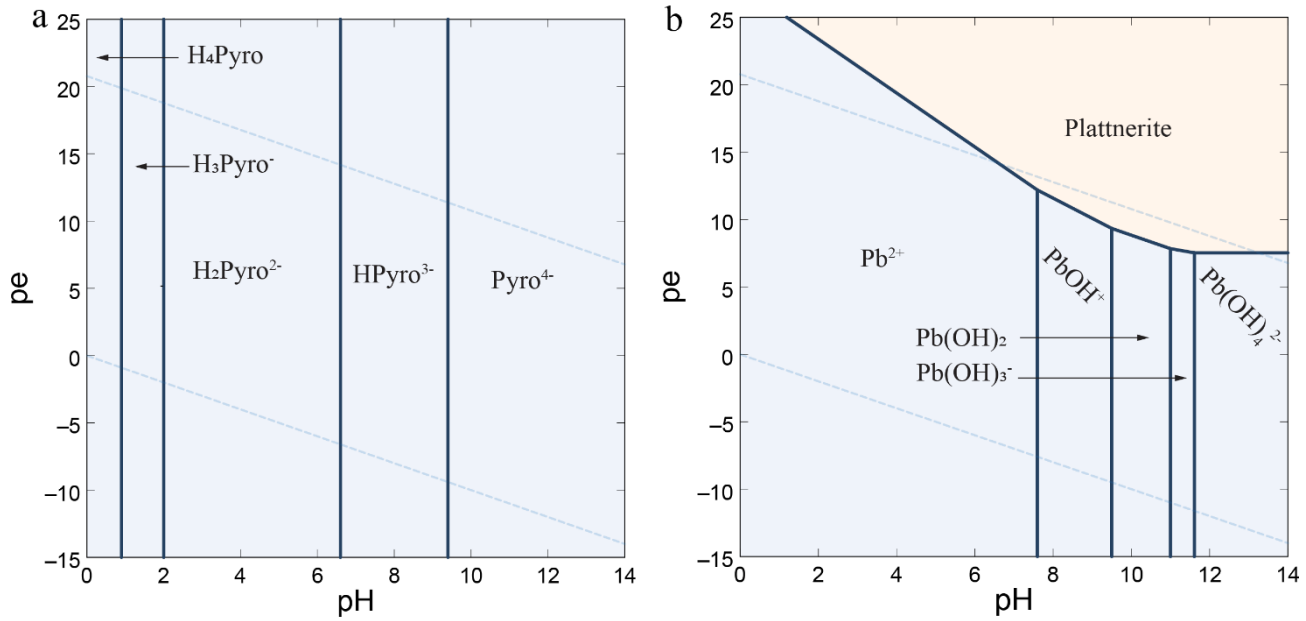

182

183 **Figure S13.** Two pe-pH diagrams of (a) PP and (b) Pb at 25 °C and 1 bar total pressure. Predominance areas
184 were calculated for conditions with 6.25 μM Pb and 500 μM PP. Light grey lines indicate the stability limits of
185 water.

Table S1. Summary of the Experimental Conditions and the Derived Thermodynamic and Kinetic Parameters.

exp[a]	pH[b]	PP (μM)	Mn(III) (μM)	Mn(II) (μM)	γ-MnOOH (μM)	PbO_2 (μM)	k_1[c,d] ($M^{-1}•h^{-1}$)	k_2[c] ($M^{-1}•h^{-1}$)	k_3[c] ($M^{-1}•h^{-1}$)	ΔG_r
					Mn(III)-PP					
1	7.00	300	50	-	-	50	9.37×10^3	N.A.[g]	N.A.	-17.74
2	7.00	500	50	-	-	50	1.08×10^3	N.A.	N.A.	-12.67
3	7.00	1500	50	-	-	50	2.60×10^2	N.A.	N.A.	-1.78
4	7.00	2500	50	-	-	50	$< 4.22 \times 10^1$	N.A.	N.A.	3.29
5	7.00	5000	50	-	-	50	$< 2.24 \times 10^1$	N.A.	N.A.	10.16
6	7.00	25000	50	-	-	50	0	N.A.	N.A.	26.12
					Mn(II)-PP					
7	7.00	300	-	50	-	50	8.51×10^2	7.94×10^3	1.98×10^4	-66.01
8	7.00	500	-	50	-	50	6.48×10^2	9.01×10^3	1.88×10^4	-67.28
9	7.00	1500	-	50	-		3.03×10^2	1.03×10^4	1.63×10^4	-70.33
10	7.00	2500	-	50	-	50	$< 5.95 \times 10^1$	4.05×10^4	5.60×10^4	-71.60
11	7.00	5000	-	50	-		$< 2.34 \times 10^1$	5.53×10^4	2.12×10^4	-73.32
12	7.00	25000	-	50	-	50	0	8.58×10^4	2.00×10^3	-77.31
					γ-MnOOH					
13	7.00	-	-	-	500	50	N.A.	N.A.	N.A.	-16.49[f]
14	7.00	2500	-	-	500	50	N.A.	N.A.	N.A.	N.A.
					Variation of pH					
15	6.00	500	50	-	-	50	4.27×10^3	N.A.	N.A.	-20.67
16	8.00	500	50	-	-	50	2.82×10^3	N.A.	N.A.	-19.53
17	6.00	500	-	50	-	50	N.A.	N.A.	N.A.	-24.77
18	8.00	500	-	50	-	50	4.66×10^3	2.78×10^3	4.74×10^3	-43.35
					Control experiments					
19	7.00	2500	-	-	-	50	N.A.	N.A.	N.A.	N.A.
20	7.00	-	-	50	-	50	N.A.	N.A.	2.45×10^3	-21.51
21	7.00	-	-	-	500	-	N.A.	N.A.	N.A.	N.A.
22	7.00	-	-	-	-	50	N.A.	N.A.	N.A.	N.A.

[a]Experiments were performed in duplicate. [b]Our previous study[2] indicated that Mn(III)-PP complex was more stable at neutral pH than at acid and alkaline pH. Therefore, pH 6, 7 and 8 were chose in this study. Excess PP automatically served as a pH buffer. Otherwise, 10 mM MOPS was used as pH buffer. [c] The rate constant (k_1, k_2, and k_3 of the reactions in eqs 1, 2, and 3) for the Mn(II)/Mn(III)-PP and PbO_2 reaction was obtained by fitting the experimental dissolved Pb and Mn(III) data using the kinetic rate expression of eqs 5 to 9. [d] For experiments with high PP:Mn ratios, eq 1 might have proceeded too slowly to constrain the kinetic model, for which we reported the upper bounds of k_1. [e]ΔG_r was normalized for every mole of electron transfer. The ΔG_r for the Mn(II)/Mn(III)-PP and PbO_2 reaction was obtained by calculating at half conversion of Mn(II)/Mn(III)-PP according to eqs 1- 3. [f]The ΔG_r for the γ-MnOOH and PbO_2 reaction (eq 4) was obtained by calculating at half conversion of PbO_2. [g]N.A.: Not applicable.

Table S2. Binding energies (BE) of surface Mn species for fitting the Mn $2p_{3/2}$ peak of the solids and the relative area of each multiplet for the surface species (All peaks were modeled as 70% Gaussian-30% Lorentzian).

Solids at the 1:10 ratio of PP to Mn(III) (Figure 6a)			
Surface species	BE (eV)	FWHM (eV)	Percent(%)
Mn(III)-O multiplet 1	640.55	1.25	15.19
Mn(III)-O multiplet 2	641.45	1.25	11.65
Mn(III)-O multiplet 3	642.06	1.25	6.84
Mn(III)-O multiplet 4	643.08	1.25	5.06
Mn(III)-O multiplet 5	644.45	1.25	2.78
Mn(III)-O overall: 40.00%			
Mn(IV)-O multiplet 1	641.8	1.25	25.32
Mn(IV)-O multiplet 2	642.82	1.25	14.18
Mn(IV)-O multiplet 3	643.70	1.25	10.89
Mn(IV)-O multiplet 4	644.83	1.25	6.58
Mn(IV)-O multiplet 5	645.90	1.25	5.32
Mn(IV)-O overall: 60.00%			
AOS:3.60		Abbe Criterion value[13]: 0.301	

Solids at the 1:50 ratio of PP to Mn(III) (Figure 6b)			
Surface species	BE (eV)	FWHM (eV)	Percent(%)
Mn(III)-O multiplet 1	640.55	1.25	9.73
Mn(III)-O multiplet 2	641.45	1.25	10.81
Mn(III)-O multiplet 3	642.26	1.25	7.84
Mn(III)-O multiplet 4	643.08	1.25	5.95
Mn(III)-O multiplet 5	644.50	1.25	3.24
Mn(III)-O overall: 36.01%			
Mn(IV)-O multiplet 1	641.81	1.25	27.03
Mn(IV)-O multiplet 2	642.90	1.25	15.95
Mn(IV)-O multiplet 3	643.80	1.25	12.16
Mn(IV)-O multiplet 4	644.88	1.25	6.76
Mn(IV)-O multiplet 5	645.90	1.25	4.86
Mn(IV)-O overall: 63.99%			
AOS:3.64		Abbe Criterion value: 0.147	

Solids at the 1:10 ratio of PP to Mn(II) (Figure 6c)			
Surface species	BE (eV)	FWHM (eV)	Percent(%)
Mn(III)-O multiplet 1	640.55	1.25	11.48
Mn(III)-O multiplet 2	641.25	1.25	11.48
Mn(III)-O multiplet 3	642.06	1.25	9.06
Mn(III)-O multiplet 4	643.08	1.25	7.25
Mn(III)-O multiplet 5	644.52	1.25	3.63
Mn(III)-O overall: 36.41%			
Mn(IV)-O multiplet 1	641.99	1.25	30.21
Mn(IV)-O multiplet 2	642.91	1.25	16.01
Mn(IV)-O multiplet 3	643.71	1.25	15.11
Mn(IV)-O multiplet 4	644.88	1.25	8.46
Mn(IV)-O multiplet 5	645.90	1.25	5.14
Mn(IV)-O overall: 63.59%			
AOS:3.64		Abbe Criterion value: 0.117	

Solids at the 1:50 ratio of PP to Mn(II) (Figure 6d)			
Surface species	BE (eV)	FWHM (eV)	Percent(%)
Mn(III)-O multiplet 1	640.55	1.25	11.11
Mn(III)-O multiplet 2	641.45	1.25	11.11
Mn(III)-O multiplet 3	642.26	1.25	8.95
Mn(III)-O multiplet 4	643.08	1.25	6.79
Mn(III)-O multiplet 5	644.45	1.25	3.70
Mn(III)-O overall: 35.25%			
Mn(IV)-O multiplet 1	641.87	1.25	30.86
Mn(IV)-O multiplet 2	642.87	1.25	16.36
Mn(IV)-O multiplet 3	643.71	1.25	15.43
Mn(IV)-O multiplet 4	644.88	1.25	8.64
Mn(IV)-O multiplet 5	645.90	1.25	5.25
Mn(IV)-O overall: 64.75%			
AOS:3.65		Abbe Criterion value: 0.200	

206

Table S3. Elemental composition (Atomic %) of solids analyzed by the EDS.

Sample Sites in Figure S9	O	P	Mn	Pb
a-1	75.66	-	-	24.34
a-2	72.92	-	-	27.08
a-3	72.98	-	-	27.02
mean	73.85	-	-	26.15
b-1	62.81	-	-	37.19
b-2	62.09	-	-	37.91
b-3	66.67	-	-	33.33
mean	63.85			36.15
c-1	18.79	10.72	0.72	69.77
c-2	15.22	10.49	1.78	72.51
c-3	17.68	11.00	0.47	70.84
mean	17.23	10.74	0.99	71.04
c-4	30.12	1.85	32.03	36.01
c-5	33.70	1.55	31.52	33.24
c-6	28.16	2.83	27.35	41.67
mean	30.66	2.07	30.30	36.97
d-1	67.00	16.83	0.00	16.16
d-2	73.25	11.76	3.03	11.96
d-3	59.13	16.15	6.33	18.39
mean	66.46	14.92	3.12	15.50
d-4	64.14	1.91	26.63	7.33
d-5	62.73	1.79	27.90	7.58
d-6	47.31	1.50	40.69	10.50
mean	58.06	1.73	31.74	8.47
e-1	66.16	1.32	24.80	7.71
e-2	66.07	1.81	24.23	7.89
e-3	67.30	1.63	23.45	7.62
mean	66.51	1.59	24.16	7.74
f-1	59.34	-	32.52	8.14
f-2	68.82	-	24.68	6.50
f-3	60.28	-	31.45	8.26
mean	62.81	-	29.55	7.63
g-1	63.22	-	28.27	8.51
g-2	64.12	-	27.26	8.63
g-3	67.27	-	25.06	7.67
mean	64.87	-	26.86	8.27
h-1	68.44	-	24.90	6.66
h-2	61.04	-	2.66	36.30
h-3	62.73	-	29.60	7.68
mean	64.07	-	19.05	16.88

Two different kinds of products were found in the experiments at pH 6, the regular flakes and irregular particles (Figure S9 c, d). The former has a composition containing more P and less Mn, which indicated the formation of lead phosphate compounds. The regular flakes were identical with the platy triclinic crystals characteristic of $Pb_2P_2O_7$.[14] The latter contained very few P and more Mn, which reflected a composition primarily containing oxides of lead and manganese. These results were confirmed by the following Raman analysis.

Table S4. Equilibrium reaction and constants relevant to the Mn thermodynamic calculations (note the direction how the reactions were written)

Species	Equilibrium Reactions	log*K* (25℃)	Reference
Mn^{3+}	$Mn^{3+} + 0.5H_2O = Mn^{2+} + H^+ + 0.25O_{2(aq)}$	4.0811	GWB Thermo_Ladder.dat
MnO_4^-	$MnO_4^- + 3H^+ = Mn^{2+} + 1.25O_2(aq) + 1.5H_2O$	20.2928	GWB Thermo_Ladder.dat
$Mn(OH)_2(aq)$	$Mn(OH)_2 + 2H^+ = Mn^{2+} + 2H_2O$	22.1962	GWB Thermo_Ladder.dat
$MnPP^{2-}$	$MnPP^{2-} = Mn^{2+} + PP^{4-}$	-6.51	Bilinski, H. Polyhedron 1983, 2 (5), 353-358
Birnessite(aq) (Mn_8O_{14}•$5H_2O$)	$Birnessite_{(aq)} + 16H^+ = 8Mn^{2+} + 3O_{2(aq)} + 13H_2O$	22.6975[a]	GWB Thermo_Ladder.dat
Birnessite	Birnessite = Birnessite(aq)	-9[a]	GWB Thermo_Ladder.dat
$MnO_2(aq)$	$MnO_{2(aq)} + 2H^+ = Mn^{2+} + 0.5O_{2(aq)} + H_2O$	7.5622[b]	GWB Thermo_Ladder.dat
Pyrolusite	Pyrolusite = $MnO_{2(aq)}$	-9[b]	GWB Thermo_Ladder.dat
$Mn(OH)_2$ (am)	$Mn(OH)_2 + 2H^+ = Mn^{2+} + 2H_2O$	15.2989	GWB Thermo_Ladder.dat
Hausmannite (Mn_3O_4)	$Hausmannite + 8H^+ = Mn^{2+} + 2Mn^{3+} + 4H_2O$	10.1554	GWB Thermo_Ladder.dat
Mn^{2+}	$Mn^{2+} + H^+ + 0.25\ O_{2(aq)} = Mn^{3+} + 0.5H_2O$	-4.0811	GWB Thermo_Ladder.dat
Birnessite (aq)	$Birnessite\ (aq) + 24\ H^+ = 8\ Mn^{3+} + 17\ H_2O + O_2(aq)$	-9.9513	GWB Thermo_Ladder.dat
$MnO_2(aq)$	$MnO_2(aq) + 3\ H^+ = Mn^{3+} + 1.5\ H_2O + .25\ O_2(aq)$	3.4811	GWB Thermo_Ladder.dat
MnO_4^-	$MnO_4- + 4\ H^+ = Mn^{3+} + 2\ H_2O + O_2(aq)$	16.2117	GWB Thermo_Ladder.dat
MnO_4^{2-}	$MnO_4^{2-} + 5\ H^+ = Mn^{3+} + 2.5\ H_2O + .75\ O_2(aq)$	28.3292	GWB Thermo_Ladder.dat
$Mn(OH)_2$	$Mn(OH)_2 + 3\ H^+ + .25\ O_2(aq) = Mn^{3+} + 2.5\ H_2O$	18.1151	GWB Thermo_Ladder.dat
Manganite (MnOOH)	$Manganite + 3H^+ = Mn^{3+} + 2H_2O$	-0.1668	GWB Thermo_Ladder.dat
Birnessite	$Birnessite + 24\ H^+ = 8\ Mn^{3+} + 17\ H_2O + O_2(aq)$	-18.9513	GWB Thermo_Ladder.dat
Hausmannite	$Hausmannite + 9\ H^+ + .25\ O_2(aq) = 3\ Mn^{3+} + 4.5\ H_2O$	6.0743	GWB Thermo_Ladder.dat
Manganite	$Manganite + 3\ H^+ = Mn^{3+} + 2\ H_2O$	-0.1668	GWB Thermo_Ladder.dat
$Mn(OH)_2(am)$	$Mn(OH)_2(am) + 3\ H^+ + 0.25\ O_2(aq) = Mn^{3+} + 2.5\ H_2O$	11.2178	GWB Thermo_Ladder.dat
$Mn(PP)_2^{5-}$	$Mn(PP)_2^{5-} + 4\ H^+ = Mn^{3+} + 2\ H_2Pyro--$	1.1	GWB Thermo_Ladder.dat

Species	Equilibrium Reactions	log*K* (25℃)	Reference
Mn^{2+}	Mn^{2+} + 1.5 H_2O + 0.25 O_2(aq) = Manganite + 2 H^+	-3.9143	GWB Thermo_Ladder.dat
Birnessite (aq)	Birnessite (aq) = 8 Manganite + H_2O + O_2(aq)	-8.6169	GWB Thermo_Ladder.dat
Mn^{3+}	Mn^{3+} + 2 H_2O = Manganite + 3 H^+	0.1668	GWB Thermo_Ladder.dat
MnO_2(aq)	MnO_2(aq) + 0.5 H_2O = Manganite + 0.25 O_2(aq)	3.6479	GWB Thermo_Ladder.dat
MnO_4^-	MnO_4^- + H^+ = Manganite + O_2(aq)	16.3785	GWB Thermo_Ladder.dat
MnO_4^{2+}	MnO_4^{2+} + 2 H^+ = Manganite + 0.5 H_2O + 0.75 O_2(aq)	28.496	GWB Thermo_Ladder.dat
$Mn(OH)_2$	$Mn(OH)_2$ + 0.25 O_2(aq) = Manganite + 0.5 H_2O	18.2819	GWB Thermo_Ladder.dat
Birnessite	Birnessite = 8 Manganite + H_2O + O_2(aq)	-17.6169	GWB Thermo_Ladder.dat
Hausmannite	Hausmannite + 1.5 H_2O + 0.25 O_2(aq) = 3 Manganite	6.5747	GWB Thermo_Ladder.dat
$Mn(OH)_2$(am)	$Mn(OH)_2$(am) + 0.25 O_2(aq) = Manganite + 0.5 H_2O	11.3846	GWB Thermo_Ladder.dat
$Mn(PP)_2^{5-}$	$Mn(PP)_2^{5-} = Mn^{3+} + 2PP^{4-}$	-30.9	Gordienko et al. 1970
MnH_2PP^+	$MnH_2PP^+ = Mn^{3+} + 2H^+ + PP^{4-}$	-21.1	Gordienko et al. 1970
$MnH_4(PP)_2^-$	$MnH_4(PP)_2^- = Mn^{3+} + 4H^+ + 2PP^{4-}$	-40.4	Gordienko et al. 1970
$MnH_6(PP)_3^{3-}$	$MnH_6(PP)_3^{3-} = Mn^{3+} + 6H^+ + 3PP^{4-}$	-59.2	Gordienko et al. 1970
$Pb(OH)_2$(aq)	$Pb(OH)_2$(aq) + 2H^+ = Pb^{2+} + 2H_2O	17.094	GWB Thermo_Ladder.dat
$Pb(OH)_3^-$	$Pb(OH)_3^-$ + 3H^+ = Pb^{2+} + 3H_2O	28.091	GWB Thermo_Ladder.dat
$Pb(OH)_4^{2-}$	$Pb(OH)_4^{2-}$ + 4H^+ = Pb^{2+} + 4H_2O	39.699	GWB Thermo_Ladder.dat
$PbOH^+$	$PbOH^+$ + H^+ = Pb^{2+} + H_2O	7.597	GWB Thermo_Ladder.dat
Plattnerite	Plattnerite + 2H^+ = Pb^{2+} + 2H_2O + 0.5 O_2(aq)	6.5601	GWB Thermo_Ladder.dat

a. Fictive Mn(III)-Mn(IV) species with activity of 10^{-9} in equilibrium with birnessite:

Birnessite + 16 H^+ = 8 Mn^{2+} + 3 O_2(aq) + 13 H_2O log*K* = 11.6975

Birnessite = Birnessite (aq) log*K* = -9

Birnessite (aq) + 16 H^+ = 8 Mn^{2+} + 3 O_2(aq) + 13 H_2O log*K* = 22.6975

b. Fictive Mn(IV) species with activity of 10^{-9} in equilibrium with pyrolusite:

246 Pyrolusite + $2H^+ = Mn^{2+} + 1/2\ O_2(aq) + H_2O$ log*K* = -1.4378

247 Pyrolusite = $MnO_{2(aq)}$ log*K* = -9

248 $MnO_2(aq) + 2H^+ = Mn^{2+} + 1/2\ O_2(aq) + H_2O$ log*K* = 7.5622

249

250 Other critical description of the Thermo_Ladder database (adapted and modified from the file header)

251 activity model: debye-huckel

252 File thermo_ladder.dat is the LLNL thermo.dat database modified to allow decoupling of the Mn(III) and Mn(IV) redox
253 states. Specifically:

254 (1) the Mn^{3+} redox species has been imported from thermo.com.v8.r6+.dat.

255 (2) a fictive Mn(IV) redox specie $MnO_2(aq)$ has been created, with a stability set to give an activity of 10^{-9} in equilibrium
256 with pyrolusite.

257 (3) reactions for the Mn(III)- and Mn(IV)-bearing minerals have been rebalanced in terms of the new redox species.

258 (4) there is a second fictive redox species of mixed Mn(III)-Mn(IV) valance state, for decoupling Birnessite.

259 (5) The pK_a constants of pyrophosphates were from McElroy, W.D.; Glass, B. Phosphorus Metabolism, Vol. I, Baltimore,
260 Johns Hopkins University Press, 1951.

References

(1) McElroy, W. D.; Glass, B., *Phosphorus Metabolism*. Johns Hopkins University Press: 1951; Vol. 1.

(2) Qian, A.; Zhang, W.; Shi, C.; Pan, C.; Giammar, D. E.; Yuan, S.; Zhang, H.; Wang, Z., Geochemical Stability of Dissolved Mn(III) in the Presence of Pyrophosphate as a Model Ligand: Complexation and Disproportionation. *Environ. Sci. Technol.* **2019,** *53*, (10), 5768-5777.

(3) Banerjee, D.; Nesbitt, H. W., XPS study of reductive dissolution of birnessite by H_2SeO_3 with constraints on reaction mechanism. *Am. Mineral.* **2000,** *85*, (5-6), 817-825.

(4) Ilton, E. S.; Post, J. E.; Heaney, P. J.; Ling, F. T.; Kerisit, S. N., XPS determination of Mn oxidation states in Mn (hydr)oxides. *Appl. Surf. Sci.* **2016,** *366*, 475-485.

(5) Bethke, C. M.; Sanford, R. A.; Kirk, M. F.; Jin, Q.; Flynn, T. M., The thermodynamic ladder in geomicrobiology. *Am. J. Sci.* **2011,** *311*, (3), 183-210.

(6) Gunary, D., Pyro phosphate in Soil; some Physico-chemical Aspects. *Nature* **1966,** *210*, (5042), 1297-1298.

(7) Wang, Z.; Giammar, D. E., Metal Contaminant Oxidation Mediated by Manganese Redox Cycling in Subsurface Environment. In *Advances in the Environmental Biogeochemistry of Manganese Oxides*, American Chemical Society: 2015; Vol. 1197, pp 29-50.

(8) Tebo, B. M.; Bargar, J. R.; Clement, B. G.; Dick, G. J.; Murray, K. J.; Parker, D.; Verity, R.; Webb, S. M., BIOGENIC MANGANESE OXIDES: Properties and Mechanisms of Formation. *Annual Review of Earth and Planetary Sciences* **2004,** *32*, (1), 287-328.

(9) Feng, X. H.; Zhu, M.; Ginder-Vogel, M.; Ni, C.; Parikh, S. J.; Sparks, D. L., Formation of nano-crystalline todorokite from biogenic Mn oxides. *Geochim. Cosmochim. Acta* **2010,** *74*, (11), 3232-3245.

(10) Le Saoût, G.; Simon, P.; Fayon, F.; Blin, A.; Vaills, Y., Raman and infrared study of $(PbO)_x(P_2O_5)_{(1-x)}$ glasses. *Journal of Raman Spectroscopy* **2002,** *33*, (9), 740-746.

(11) Yang, P.; Post, J. E.; Wang, Q.; Xu, W.; Geiss, R.; McCurdy, P. R.; Zhu, M., Metal Adsorption Controls Stability of Layered Manganese Oxides. *Environ. Sci. Technol.* **2019,** *53*, (13), 7453-7462.

(12) Julien, C. M.; Massot, M.; Poinsignon, C., Lattice vibrations of manganese oxides. *Spectrochimica Acta Part A: Molecular and Biomolecular Spectroscopy* **2004,** *60*, (3), 689-700.

(13) Hesse, R.; Chassé, T.; Streubel, P.; Szargan, Error estimation in peak‐shape analysis of XPS core‐level spectra using UNIFIT 2003: how significant are the results of peak fits? *Surface and Interface Analysis: An International Journal devoted to the development and application of techniques for the analysis of surfaces, interfaces and thin films* **2004,** *36*, (10), 1373-1383.

(14) Lytle, D. A.; White, C.; Schock, M. R., Synthesis of Lead Pyrophosphate, $Pb_2P_2O_7$, in Water. *Microsc. Microanal.* **2008,** *14*, (4), 335-341.